Recovery of the Human Striatal Signal in a Slice Oriented Positron Emission Tomograph

Vesna Sossi, Kenneth R. Buckley, Barry J. Snow, James E. Holden, K. Scott Morrison, Brian D. Pate and Thomas J. Ruth

University of British Columbia/TRIUMF Positron Emission Tomography, Vancouver, British Columbia, Canada and Department of Medical Physics, University of Wisconsin, Madison, Wisconsin

The human striatum is small enough for partial volume effects to be important when imaged in positron tomographs with slice widths 10 mm or greater. The combination of inter-slice distance and slice width in such tomographs results in an axial undersampling of the striatal activity which introduces the additional problem of variation of axial recovery as a function of position of the striatum along the tomograph axis. Using striatal phantoms, we have developed a method that corrects the recovered striatal signal to a maximum value equivalent to that measured when the object is centered with respect to a slice. This makes the recovery independent of the axial position of the striatum. The method also provides an estimate of the total striatal activity by integrating the axial image intensity distribution along the tomograph axis. The method is able to detect and correct for relative axial tilt of the left and right striatum. We applied it to 26 human [^{18}F]-6-L-fluorodopa scans and obtained an average uptake rate constant k value of 0.25 ± 0.05 ml/min/striatum and a left to right k value percentage asymmetry of 0.1% ± 6.3%.

J Nucl Med 1993; 34:481–487

The finite resolution of PET tomographs causes an underestimation in the measurement of the radiotracer intensity for objects comparable to or smaller than the tomograph resolution element (partial volume effect) (*1*). An inter-slice distance larger than about half the size of an imaged object further introduces a variation of the axial contribution to the partial volume effect caused by axial undersampling (*2*). As a consequence, the amount of signal recovered is a function of the object position with respect to the center of a slice and reaches a minimum value when the object is centered between two slices (*2*).

The human striatum extends about 2 cm in the axial direction of the tomograph. Its image usually appears in three adjacent slices in a tomograph with a slice width of 10–15 mm and a similar slice-center-to-slice-center separation. The combination of the values of these parameters is such that the recovery varies significantly along the tomograph axis. Striatal activity measured from a single slice is therefore not necessarily representative of either the true concentration of the tracer in the striatum or the total tracer in that region.

To estimate consistently the true concentration and the total striatal activity, we have developed a method that overcomes the dependence of the signal recovery on axial position as well as corrects for the relative axial tilt of the two striata. The method is based on defining axial image intensity distribution curves for the left and right striatum separately. These are obtained by fitting Gaussian curves to image intensity samples obtained by scanning in three axial positions separated by approximately a third of the inter-slice distance. The ratios between the image intensity measured in the selected slice and the peak of the axial activity distributions are then used to correct the measured values to the peak values. The total image intensities for the left and right striatum are estimated from the integral along the tomograph axis of the axial image intensity distributions.

This method is applicable to any situation where the results suffer from undersampling. In the case of human and animal studies, this approach is applicable to situations in which the poorly recovered anatomical structure is distinguishable at high contrast from the surrounding tissue and there is a relatively stable time course of the radiotracer. The method was validated with phantom studies and then applied to 26 human [^{18}F]-6-L-fluorodopa scans (age range 45 ± 23 yr).

METHODS

Striatal Phantom Studies

The scans were performed on the UBC/TRIUMF PETT-VI tomograph (*3*). The PETT-VI has four rings of detectors yielding four "true" and three "cross" slices with a slice-center-to-slice-center separation (interslice distance) of 14.4 mm. The average in-plane spatial resolution is 9.2 mm FWHM and the average slice width is 11.6 mm FWHM. For this tomograph, the slice spacing is larger than the slice width, which amplifies the undersampling problem.

Two glass human striatum phantoms were constructed using

Received Apr. 24, 1992; revision accepted Oct. 14, 1992.
For correspondence or reprints contact: Vesna Sossi, TRIUMF 4004 Westbrook Mall, Vancouver, BC, V6T 2A3 Canada.

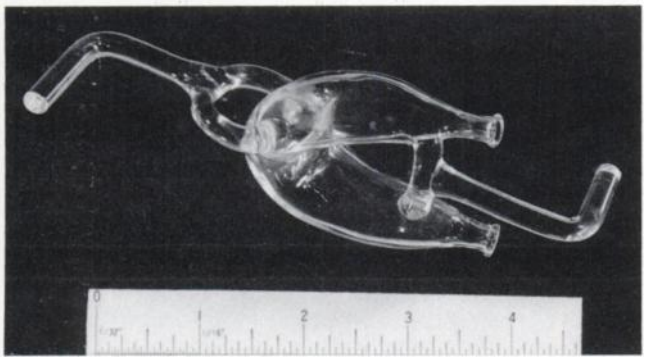

FIGURE 1. Glass striatal phantom. The total volume is about 10 ml.

a postmortem specimen as a model (Fig. 1). The phantoms had two compartments with volumes and dimensions similar to the caudate and putamen, the two main nuclei that form the striatum. Four series of measurements were then performed with only the last series using both striatal phantoms.

For all studies, other than those performed with phantoms in air, transmission scans were performed with a ring source containing ^{68}Ge to permit a measured correction for attenuation. The transmission scan was substituted by a blank scan performed with the ring source for the phantom studies performed in air.

In the first series, we defined the tomograph response to the striatal phantom signal. One phantom was filled with an aqueous solution containing approximately 2.5 MBq of ^{18}F activity and suspended in air. The phantom was placed at about 2 cm from the axial midline to simulate the position of the striatum within the human brain. The phantom was then scanned in 30 axial positions 1 mm apart. At each position, a 1-min scan was performed and the images reconstructed. The total number of events in a region of interest (ROI) totally encompassing the striatal phantom image was recorded for each step and corrected for radioactive decay.

The second series of experiments was designed to investigate the effect of background activity and consequently contrast on the tomograph response to the striatal signal. The phantom was placed in a cylindrical phantom, 20 cm diameter, filled with an aqueous ^{18}F solution to simulate the surrounding medium in brain scans. The concentration ratio between the background activity and the activity in the striatal phantom was approximately 1:10. A similar sequence of 30 scans was performed. Transmission scans were performed at each axial location and the images reconstructed. ROIs were placed on the striatal phantom images as before and additional ROIs were placed on the uniform background. The total number of events recorded in each ROI was corrected for radioactive decay.

Third, we investigated the effect of axial orientation of the striatum on the measurement of the striatal signal. The phantom was rotated along the sagittal axis by 20° and scanned in air. An analogous sequence of 30 scans was performed and treated as above.

The fourth series of experiments was performed to test the sensitivity of the method for the detection of axial tilt between the two striata due to head tilt, etc. Both striatal phantoms were filled with an aqueous solution containing about 2.1 MBq of ^{18}F activity and suspended on parallel rods extending axially throughout the field of view (FOV). The phantoms, surrounded by air, were positioned in the center of the FOV about 5 cm apart radially to simulate the human inter-striatal distance. One phantom was moved axially with respect to the other in five steps 4 mm apart to simulate various degrees of axial tilt. For each relative position of the two phantoms, three scans were taken with the second and third being 7 and 10.5 mm apart from the first, respectively. The collected data were analyzed as before.

Human Studies

On the basis of the results of the phantom studies (see Results), we modified our human scanning protocol for human FD studies (*3*). In order to optimally position the subject for the emission scans, two transmission scans were first performed at positions 7 mm apart axially and sagittal profiles were reconstructed from the data. A "home" position in which the dynamic emission scan sequence would be performed was chosen from the transmission scan results to be that in which the striata appeared to be better centered with respect to a "true" slice. Seventy minutes after FD injection, when the striatal signal plateaued, emission scans taken at two additional axial positions were interleaved with those taken in the home position yielding a total of thirteen 10-min emission scans. The resulting sequence is described in Table 1.

The resulting axial sampling was thus increased by a factor of three as determined from the phantom studies (see Results), and unequally spaced with one 7-mm and two 3.5-mm steps (Figs. 3 and 4). The transmission scan taken in the nearest axial position to the respective emission scan was used in the reconstruction of the images. The maximum axial displacement between an emission and a transmission scan was 3.5 mm which, we found, did not introduce a significant error.

Background and striatal ROIs were placed on three adjacent slices. The size of the striatal ROIs was about 10 cm^2 to ensure inclusion of most striatal activity, while the size of the ROIs placed on the cortical region (background ROI) was about 12 cm^2 (*3*).

ANALYSIS

Phantom Studies

Figure 2 shows data from the scanning of a single striatal phantom in air (first phantom study) and demonstrates the basic approach that is used to analyze these data and all subsequent phantom data and which in turn provides the basis for the analysis of the human data. In Figure 2A, the values of image intensity summed over the

TABLE 1
Transmission and Emission Scan Locations and Sequence

	Emission scan number	Transmission scan number
Position 1 (home)	1-7, 9, 11	T1 or T2
Position 2	8, 10, 12	T2 or T1
Position 3	13	—

Position 1 and 2 are 7 mm apart; position 3 is either in between positions 1 and 2 or 3.5 mm on either side.

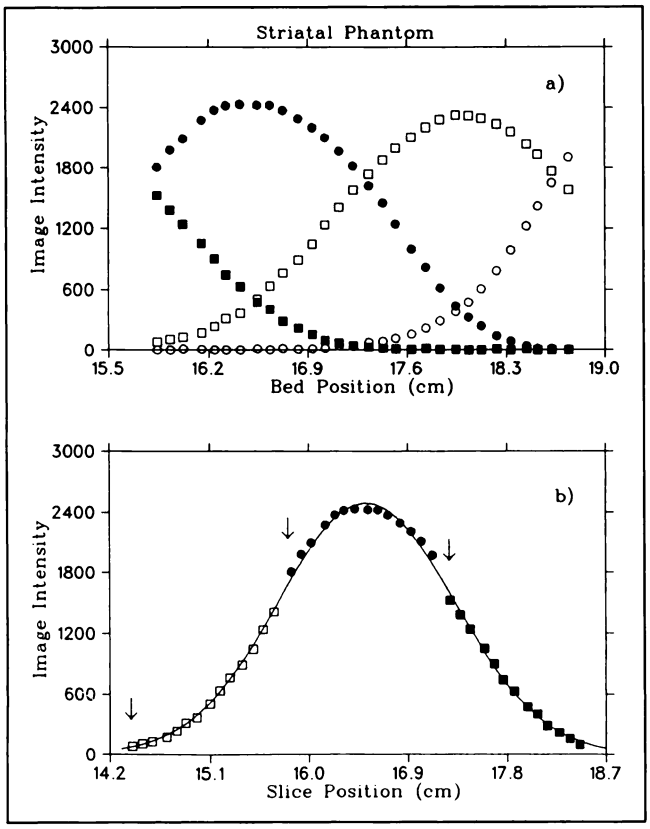

FIGURE 2. Axial distribution data from the striatal phantom scanned in air. (a) Image intensity recorded in each slice as a function of bed position along the tomograph axis, with an arbitrary offset. Intensity units are proportional to tomograph cps/ROI. "Cross" (circles) and "true" (squares) slices show approximately equal response. The phantom is detectable in three slices except when it is located exactly between two slices. (b) An arbitrary subset of the same data, chosen so that the measurements do not spatially overlap with the appropriate axial offsets included. The symbols refer to the same slices as in a. Solid line is the Gaussian curve fit to the data (see text). The arrows indicate an example of image intensity recorded in three slices during the same scan.

pixels in the striatal ROI are plotted as a function of bed position at which the data were collected. Each point on the abscissa is thus associated with four plotted points showing the response to the striatal phantom in each slice. The phantom always produced an image in three adjacent slices. As a result, three samples of the axial intensity distribution were obtained for each scanning position. Figure 2B shows a subset of the data from the first three slices plotted in Figure 2A, which were chosen so that the measurements would not spatially overlap. The data from the second of the three slices were replotted with their original abscissa values. However, data from the first slice were shifted by one interslice distance (14.4 mm) to higher bed position values and those from the third slice were shifted by the same interval to lower values in order to bring them into registration with respect to the object. The resulting axial image intensity distribution had a Gaussian shape and was fitted with a Gaussian function of the form:

$$y = y_{peak} \times \exp\left(-(x - x_0)^2/c\right), \qquad \text{Eq. 1}$$

where y_{peak} is the peak amplitude, x_0 is the center position of the activity distribution of the imaged phantom and c is a function of the FWHM of the curve ($c = FWHM^2/(-4 \ln(0.5))$). c depends on the object size and axial slice width. These three parameters were allowed to vary for the fit.

In the case of the striatal phantom scanned in a water medium, the area of the background ROI was normalized to the area of the striatal ROI and this total background intensity was subtracted from the total measured intensity in the striatal ROI. This procedure was used to reproduce the analysis used in human studies where the specific striatal activity is extracted from the intensity measured in the ROI around the striatum by subtraction of "background" cortical activity (*3*) (see Results; Human Studies). Again the data obtained in the above described slice positions were fitted with the function of Equation 1 and the same three parameters determined.

In the fourth study where both phantoms were imaged, separate ROIs were placed around the two phantom images. Each series of three scans related to the same axial displacement of the two phantoms and yielded nine samples (3 slices × 3 bed positions) of the axial activity distribution. The image intensities were plotted as a function of slice position as before and Gaussian curves (Equation 1) were fitted to the data of each striatal phantom.

Human Studies

The analysis of the FD studies performed in our center is described by Martin et al. (*3*). The goal of this analysis is not to estimate mass-specific radioactivity concentrations, but rather the total specific signal from the whole striatum. This approach may provide an advantage over the alternative of determining the highest radiotracer concentration in the striatum, as the placement of ROIs on the images can be performed more objectively. The nonspecific striatal activity is accounted for by background correction on the assumption that the nonspecific striatal activity is comparable to the average cortical activity. The total, rather than average, pixel value from the ROIs placed on the cortical region after correction for any differences in region area is subtracted from the total summed pixel value in each striatal region for each slice. The resulting difference value represents the mean specific striatal radioactivity concentration times the number of pixels in each striatum. In the approach reported here, the axial direction is regarded as a third image dimension. If the axial samples are sufficiently close together, then integration over the axial direction with proper dimensional scaling, followed by multiplication by the trans-

verse pixel area provides the desired estimate of the total radioactivity signal arising from the striatal structures.

In the determination of the axial intensity distribution of the imaged striata, only those scans that were performed later than 70 min after injection when the striatal image intensity became relatively stable were used (scans 8–13). Six scans in the three above scanning positions yielded 18 (6 × 3) samples of the axial activity distribution in nine different axial locations (see Methods). These data were analyzed via a method analogous to that employed for the striatal phantom data.

RESULTS

Phantom Studies

The results of the first phantom study are summarized in Figures 2A and 2B. Figure 2A shows that the response from a "true" (squares) and a "cross" (circles) slice is approximately the same in the PETT-VI and the variation of recovery with axial position is evident. A minimum of recovery, about 70% of the peak recovery, occurred when the phantom was located midway between the center of two slices, which is in agreement with previous studies (*2*). The FWHM of the Gaussian curve (Equation 1) fitted to the data in Figure 2B (see Analysis) was found to be 1.8 cm.

The results of the second study, where the striatal phantom was immersed in an aqueous background medium of lower activity concentration, did not differ from those of the first study demonstrating that the presence of such a background and scattering medium did not significantly influence the axial intensity distribution.

In the third study, where the striatum was rotated along the sagittal axis by approximately 20°, the FWHM of the curve increased to 1.9 cm, confirming the expectation that the same FWHM could not be used for all PET measurements. In all cases, the Gaussian curve provided a good fit to the data, confirming that the tomograph resolution obscures structural details of the striatal phantom.

Correction Method. The consistent Gaussian shape of the axial image intensity profile was the key to the development of the correction method. A reliable fit of the axial image intensity distribution was achieved with a three-fold increase in axial sampling, yielding nine (3 slices × 3 bed positions) axial samples. The nine samples were obtained by scanning the phantom in three positions separated by approximately a third of the interslice distance. The fitting procedure determined the three variable parameters, y_{peak}, x_0 and c, and thus completely defined the axial image intensity profile y (Equation 1). Once the Gaussian curve was defined, the image intensity measured in any slice (I_{meas}) could be corrected to the peak value (I_{corr}) by multiplying the measured value by the ratio between the peak value of the curve and the value of the distribution calculated at the position of the selected slice [Correction Factor 1 (CF1)].

$$CF1 = y_{peak}/y(\text{selected slice})$$

$$I_{corr} = I_{meas} \times CF1.$$

A similar approach for the correction to the maximum intensity in the case of a single slice was described by Doudet et al. (*5*) and suggested by Links (*6*). The same axial image intensity distribution was used to estimate the total striatal activity by calculating the area under the curve.

Once the distribution was obtained, the image intensity measured in a slice (I_{meas}) could be corrected to the integral value (INTEG) by multiplying the measured value by the ratio of the area underneath the curve and the value of the image intensity distribution calculated at the position of the selected slice [Correction Factor 2 (CF2)].

$$CF2 = \text{area}/y(\text{selected slice})$$

$$INTEG = I_{meas} \times CF2.$$

This correction of the measured image intensity in a slice to the area underneath the curve will be henceforth referred to as the *integration method.*

Axial Tilt. The fourth series of experiments was designed to test the ability of the method to detect and correct for relative axial tilt of the two striata. The axial step obtained from the relative peak positions was 4.24 ± 0.68 mm, which agrees well with the 4 mm axial step used in the experiment (Table 2). The same series of experiments confirmed the reliability of the method by comparing the values of the areas underneath the Gaussian curves obtained for each relative position of the two phantoms. The standard deviation of the values of the areas under the Gaussian curves related to the moved phantom was 3%, indicating a consistent estimate of total

TABLE 2
Comparison Between the Measured Relative Position of the Two Striatal Phantoms and the Shift of Axial Activity Distribution Peaks Expressed in Millimeters

$(Z_{S1} - Z_{S2})^*$	$(\Delta Z)_{measured}$	$(peak_{S1} - peak_{S2})^\dagger$	$(\Delta Z)_{peak}$
−8		−9.23	
−4	4	−3.99	5.24
0	4	0.00	3.98
4	4	3.92	3.92
8	4	7.75	3.83
Average $(\Delta Z)_{peak}$			4.24 ± 0.68

*Relative axial distance between the two striatal phantoms S1 and S2.

†Relative axial distance of the peaks of the axial activity distributions of the two striatal phantoms.

activity while the standard deviation of the values of the areas associated with the stationary phantom was 1%.

Human Studies

Integration Method Applied to Human Studies. The axial activity distribution was determined by fitting Gaussian curves (Equation 1) to the data as in the striatal phantoms studies. The values x_0, y_{peak} and c were determined for each striatum separately. The CF2 was determined from the slice that gave the highest yield in the home position. Since the shape of the Gaussian curve is only dependent on the object size for a given tomograph, the same correction factor could be applied to all scans that were part of the dynamic sequence, yielding for each scan (i) a scaled area:

$$INTEG_i = \text{area} \times ((I_{meas})_i/y(\text{selected slice})). \quad \text{Eq. 2}$$

CF2 and CF1 are listed in Table 3. Typical results from a study of a human subject are presented in Figures 3 and 4. The background-corrected striatal image intensity in each slice is plotted as a function of slice position along the tomograph axis for all six scans used in the determination of the axial striatal image intensity distribution. In each case, the home position (dark squares) was not at the center of a tomograph slice demonstrating the need for correction for position. The eighteen samples do not always appear on the graph since in some cases the image intensity in the striatal ROIs of the slices close to the edge of the striatum are comparable to the intensity values in the background ROIs, possibly yielding a corrected striatal image intensity less than zero due to statistical effects.

The analysis performed on 26 normal subjects yielded an average FWHM of the fitted Gaussian curves of 1.9 ± 0.2 cm, a value consistent with that obtained from the phantom studies.

Striatal Uptake Rate Constant k Values. The values of the striatal FD uptake rate constant k calculated from data analyzed with the integration method are presented in Table 3. The k value averaged over the left and right striatum is 0.25 ± 0.05 ml/min/striatum. With a typical human striatal size of 13 ml (*7*), this value is equivalent to 0.019 ± 0.004 ml/min/g, which is consistent with the values reported by others (*8*).

TABLE 3
Correction Factors and Uptake Rate Constant k Values

Subject no.	$CF1_L$*	$CF1_R$*	$CF2_L$†	$CF2_R$†	$(k_L)_{int}$‡	$(k_R)_{int}$‡	k_L§	k_R§
P1	1.03	1.04	1.97	2.20	0.36	0.28	0.87	0.54
P2	1.08	1.11	1.79	2.06	0.25	0.26	0.60	0.59
P3	1.00	1.00	1.78	1.96	0.26	0.26	0.61	0.54
P4	1.03	1.08	1.71	1.72	0.16	0.14	0.35	0.32
P5	1.11	1.00	1.82	1.65	0.26	0.27	0.63	0.71
P6	1.19	1.21	1.89	2.49	0.27	0.29	0.50	0.50
P7	1.06	1.01	2.69	2.29	0.26	0.25	0.56	0.54
P8	1.01	1.02	1.72	1.73	0.29	0.27	0.82	0.64
P9	1.55	1.17	2.45	2.21	0.14	0.14	0.36	0.36
P10	1.02	1.11	1.71	1.92	0.30	0.25	0.77	0.55
P11	1.10	1.25	2.26	2.39	0.28	0.28	0.66	0.64
P12	1.10	1.14	2.19	2.20	0.29	0.30	0.65	0.66
P13	1.10	1.00	2.57	2.49	0.30	0.30	0.73	0.67
P14	1.01	1.01	1.99	1.80	0.25	0.23	0.62	0.54
P15	1.00	1.05	1.89	1.82	0.24	0.24	0.45	0.50
P16	1.06	1.18	2.13	2.41	0.17	0.26	0.37	0.47
P17	1.31	1.25	2.86	2.75	0.25	0.27	0.56	0.55
P18	1.00	1.02	2.31	2.40	0.22	0.21	0.47	0.37
P19	1.00	1.05	2.04	1.93	0.21	0.26	0.38	0.59
P20	1.52	1.44	2.87	2.72	0.21	0.22	0.49	0.53
P21	1.03	1.01	2.13	2.09	0.27	0.24	0.62	0.54
P22	1.07	1.00	2.42	1.99	0.27	0.25	0.58	0.54
P23	1.05	1.01	2.02	1.99	0.29	0.31	0.48	0.69
P24	1.02	1.00	2.37	2.26	0.26	0.24	0.47	0.46
P25	1.08	1.03	2.00	1.86	0.21	0.22	0.48	0.47
P26	1.08	1.02	2.48	2.20	0.29	0.29	0.68	0.68
Average								

*Correction Factor 1 left and right (see text).
†Correction Factor 2 left and right (see text).
‡k values obtained with the integration method (left and right).
§k values obtained with the method in Reference 6 (left and right).

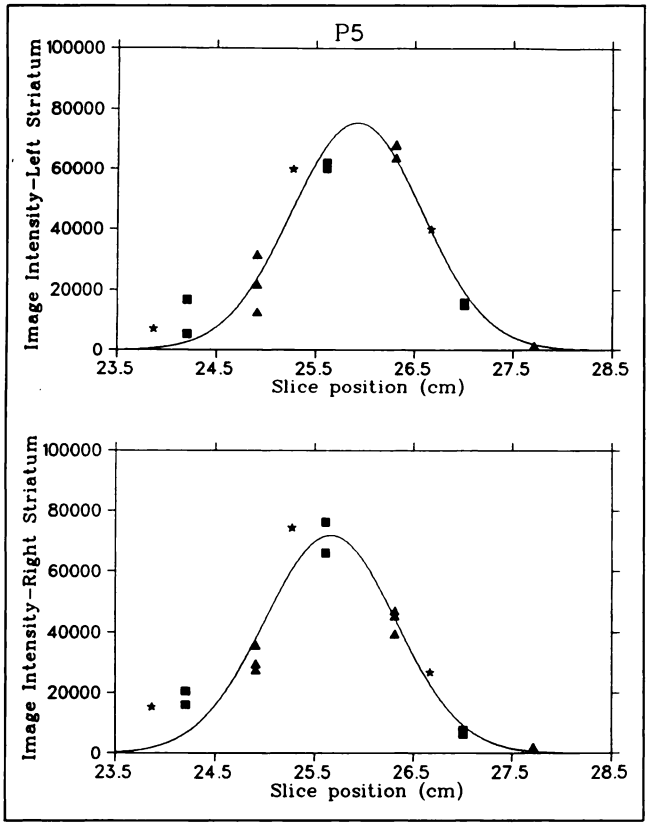

FIGURE 3. Image intensity from a human FD study for the left and right striatum. The three scanning positions are separated by 3.5 and 7 mm. Each symbol indicates the image intensity measured in each of the three slices in the scans performed in the same axial position (see Methods). Dark squares represent the image intensity measured when the scans were performed in the "home" position. Missing points indicate an uncorrected striatal image intensity lower than the corresponding background image intensity (see Analysis). The intensity units are proportional to tomograph counts/sec/ROI. The x-axis offset is arbitrary. The "home" position has a different offset with respect to the intensity distribution peak for the left and right striatum indicating the presence of tilt.

Side-to-side k Value Differences. The average value of the percentage difference between the left and right striatum k value [% Diff = (L − R)/(L + R)] was 0.1% ± 6.3%. This value is compatible with zero, the expected value, since the left and right k values are expected to be the same for normal subjects. The absolute value of the percentage difference, related to the skewedness of the distribution and used in a previous study (*9*) as a possible variable that might discriminate between normal and affected subjects, was 4.1% ± 4.8%.

Comparison to the Method by Martin et al. In the method described by Martin et al. (*3*), striatal and background ROIs analogous to the ones used with the integration method were placed on two slices only. Two background corrected striatal image intensities (see Analysis) from the two slices were then summed together with empirical scaling factors that accounted for relative sensitivity of a cross slice with respect to a true slice. On the basis of our results we set those factors to one (Fig. 2).

The average k value obtained with the method of Martin et al. (*3*) was 0.56 ± 0.12 ml/min/striatum. The difference between the k average value obtained with the integration method 0.25 ± 0.05 ml/min/striatum and the value obtained using this method by Martin et al. results from the fact that this latter method did not convert from counts/voxel to concentration. The percentage difference between the left and right striatum k value was found to be 3.0% ± 9.2% which, assuming the true asymmetry distribution to be a normal distribution for a healthy population, differs from the value obtained from the integration method at a p level of 0.08. The absolute value of the percentage difference between the left and right striatum k value obtained with this method was found to be 6.1% ± 6.9%. This variable exhibited a significantly larger variance ($p < 0.01$) when calculated from the k values obtained with this latter method as compared to the results obtained with the integration method, which confirms that the integration method provides a better correction for left-right asymmetry due to subject tilt.

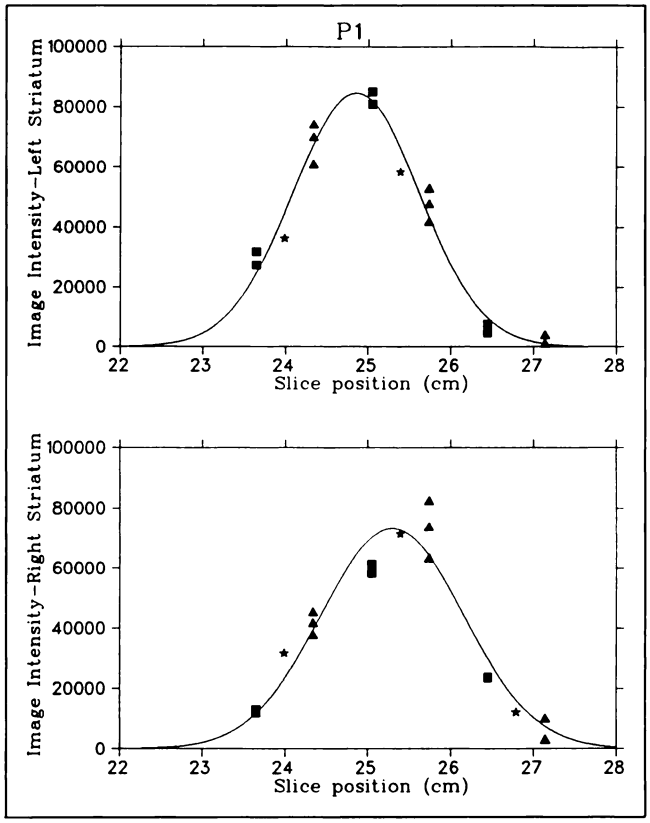

FIGURE 4. FD study of a different subject presented as in Figure 3. The scanning positions here are separated by 3.5 mm. Note that the study position falls on opposite sides of the intensity distribution peak for the left and right striatum, again indicating the presence of a tilt.

DISCUSSION AND CONCLUSION

Variation of axial recovery is a source of uncertainty when comparing intersubject data as well as when repeatedly scanning the same subject. Accurate repositioning is not always possible and usually difficult; even a small difference in the axial position of the striata can introduce artificial variations in the results. This method provides a simple solution to that problem that only adds one 10-min scan to the standard protocol (*3*). The method can be applied either to define the concentration that would have been obtained had the object been centered with respect to a slice (CF1) or to estimate the total striatal activity (CF2). Object size information is also included in this last correction factor since the FWHM of the Gaussian curve depends on the size of the imaged object.

An additional source of uncertainty in the results is due to possible tilt of the subject's head. A difference in the measured striatal image intensities between the left and right striata thus cannot necessarily be attributed to asymmetric FD uptake unless tilt can be defined. This method is able to detect tilt by defining the left and right axial intensity distribution curves separately (Figs. 3, 4). In the presence of tilt, the home positions for the left and right striatum have different offsets from the peak of the curve which results in different correction factors CF1 and CF2 for the left and right side. The correction factor CF1, for example, may differ by as much as 24% (see P9 in Table 3).

In summary, we have developed a solution to the problem of axial recovery variations along the tomograph axis, thus overcoming a dependence on signal recovery of axial position. The correction is applied separately to the left and right striatal images, thus correcting for possible tilt and functional differences between the striata. In human and animal studies, this method can be applied when using radiotracers with a relatively stable time course. This method can be used in any situation where the object size combined with the tomograph slice width and spacing hampers a consistent estimate of concentration or total activity.

ACKNOWLEDGMENTS

The authors wish to thank Dr. Michael Adam and Salma Jivan for the preparation of radiotracers; Poppy Schofield, Teresa Dobko and Sandy Cooper for help with the scanning protocols; and Dr. Michael Cordes with the analysis. This work was supported by a Program Grant from the Medical Research Council of Canada.

REFERENCES

1. Hoffman EJ, Huang SC, Phelps ME. Quantitation in positron emission computed tomography. *J Comp Assist Tomogr* 1979;3:229–308.
2. Miller TR, Wallis JW, Grothe RA Jr. Design and use of PET tomographs: the effect of slice spacing. *J Nucl Med* 1990;31:1732–1739.
3. Evans B, Harrop R, Heywood D, et al. Engineering developments of the UBC-TRIUMF modified PETT VI positron emission tomograph. *IEEE Trans Nucl Sci* 1983;NS-30:707–710.
4. Martin WRW, Palmer MR, Patlak CS, Calne DB. Nigrostriatal function in humans studied with positron emission tomography. *Ann Neurol* 1984;26: 535–542.
5. Doudet DJ, Miyake H, Finn RT, et al. 6-^{18}-F-L-DOPA imaging of the dopamine neostriatal system in normal and clinically normal MPTP-treated rhesus monkeys. *Exp Brain Res* 1989;78:69–86.
6. Links JM. The influence of positioning on accuracy and precision in emission tomography. *J Nucl Med* 1991;32:1252–1253.
7. Pasik P, Pasik T, DiFiglia M. The internal organization of the neostriatum in mammals. In Divac I, Oberg RGE, eds., *The neostriatum.* New York: Pergamon Press; 1978:5–36.
8. Huang S-C, Yu D-C, Barrio JR, et al. Kinetics and modeling of L-6-[^{18}F]Fluoro-dopa in human positron emission tomographic studies. *J Cereb Blood Flow Metab* 1991;11:898–913.
9. Cordes M, Sossi V, Snow BJ, Ruth TJ, Calne D. Quantitative measurements of the striatal [^{18}F]-L-dopa rate constant k_i and its side to side difference in Parkinsonism plus disorders using PET. *J Neuroimaging* 1992: in press.